Journal of Experimental Botany, Vol. 62, No. 15, pp. 5453–5462, 2011
doi:10.1093/jxb/err222 Advance Access publication 9 August, 2011
This paper is available online free of all access charges (see http://jxb.oxfordjournals.org/open_access.html for further details)

Journal of Experimental Botany
www.jxb.oxfordjournals.org

RESEARCH PAPER

Aluminium localization in root tips of the aluminium-accumulating plant species buckwheat (*Fagopyrum esculentum* Moench)

Benjamin Klug, André Specht and Walter J. Horst*

Institute of Plant Nutrition, Leibniz University Hannover, Faculty of Natural Science, Herrenhäuser Strasse 2, D-30419 Hannover; Germany

* To whom correspondence should be addressed. E-mail: Horst@pflern.uni-hannover.de

Received 25 March 2011; Revised 20 June 2011; Accepted 20 June 2011

Abstract

Aluminium (Al) uptake and transport in the root tip of buckwheat is not yet completely understood. For localization of Al in root tips, fluorescent dyes and laser ablation inductively coupled plasma mass spectrometry (LA-ICP-MS) were compared. The staining of Al with morin is an appropriate means to study qualitatively the radial distribution along the root tip axis of Al which is complexed by oxalate and citrate in buckwheat roots. The results compare well with the distribution of total Al determined by LA-ICP-MS which could be reliably calibrated to compare with Al contents by conventional total Al determination using graphite furnace atomic absorption spectrometry. The Al localization in root cross-sections along the root tip showed that in buckwheat Al is highly mobile in the radial direction. The root apex predominantly accumulated Al in the cortex. The subapical root section showed a homogenous Al distribution across the whole section. In the following root section Al was located particularly in the pericycle and the xylem parenchyma cells. With further increasing distance from the root apex Al could be detected only in individual xylem vessels. The results support the view that the 10 mm apical root tip is the main site of Al uptake into the symplast of the cortex, while the subapical 10–20 mm zone is the main site of xylem loading through the pericycle and xylem parenchyma cells. Progress in the better molecular understanding of Al transport in buckwheat will depend on the consideration of the tissue specificity of Al transport and complexation.

Key words: Aluminum, Al accumulator, Al–organic acid complex, *in situ* Al quantification, laser ablation ICP-MS, lumogallion, morin, xylem loading.

Introduction

Organic acids play a major role in detoxifying aluminium (Al) in the root tip apoplast (Al resistance by Al exclusion) or within the symplast of roots and shoots (Al tolerance, Al accumulation) (Ma *et al.*, 1998; Klug and Horst 2010*a*, *b*). These symplastic detoxification, compartmentation, and translocation are the most important Al tolerance-mediating processes in Al-accumulating plant species. However, these processes require Al transport through at least one membrane. Currently knowledge concerning this passage of Al through biological membranes is limited and not completely understood. These shortcomings may be primarily ascribed to the complex aqueous coordination chemistry of Al, its high affinity for O_2 donor compounds, and the lack of appropriate stable isotopes (Taylor *et al.*, 2000). Therefore, Al has often been detected by fluorescence microscopy and spectrometry. The fluorochromes morin and lumogallion form stable complexes with Al (Kataoka *et al.*, 1997; Vitorello and Haug, 1997). The fluorescence emission of the chromophore–Al complexes has frequently been used for the determination and quantification of Al in freshwater, generally in biological samples, and extensively for the localization of Al in plant tissues, particularly in root tips (Levesque *et al.*, 2000; Tanoi

Abbreviations: Cit, citrate; LA-ICP-MS, laser ablation inductively coupled plasma mass spectrometry; Mal, malate; Ox, oxalate.

© 2011 The Author(s).

This is an Open Access article distributed under the terms of the Creative Commons Attribution Non-Commercial License (http://creativecommons.org/licenses/by-nc/2.5), which permits unrestricted non-commercial use, distribution, and reproduction in any medium, provided the original work is properly cited.

et al., 2001; Ahn et al., 2002; Gutierrez and Gehlen, 2002; Eticha et al., 2005; Jones et al., 2006; Ščančar and Milačič, 2006; Babourina and Rengel, 2009).

The formation of the morin–Al complex is strongly influenced by the binding stage of Al. The precise binding conditions of lumogallion are currently unknown. The correct assessment of the specific conditions underlying Al–dye complex formation is of particular importance, especially in the case of Al-accumulating plant species such as buckwheat, where Al is thought to be bound to organic acids in the root apoplast and plant tissues.

The targeted staining of Al within roots of buckwheat could provide further information about Al uptake and transport in the root tissue. However, this requires information on specific dye–ligand interactions and subsequent responses in fluorescence emission. Browne et al. (1990*a*, *b*) stated that morin is a reagent which reliably complexes Al, with 'minimized disturbance'. In that study, the fluorescence of the Al–morin complex was directly related to Al^{3+} and Al hydroxy complexes, indicating that morin forms complexes only with inorganic monomeric Al species but not with Al–organic acid complexes (Lian et al., 2003). The precise Al–morin complex formation and underlying stability constants remained unclear for a long time. It was reported that morin detects cell wall-bound Al (Ahn et al., 2002), but Eticha et al. (2005) unequivocally showed that morin could not stain cell wall-bound Al. The results of Eticha et al. support the conclusion that morin is not able to stain Al in high stability complexes (Lian et al., 2003).

The aim of this study was to investigate in depth the limitations and prospects of morin and lumogallion for staining Al in buckwheat utilizing oxalate and citrate as the main Al complexors in the plant tissue. Furthermore, the results on the Al distribution based on Al staining with dyes should be compared with the determination of total Al concentrations measured by laser ablation inductively coupled plasma mass spectrometry (LA-ICP-MS). It was expected that the localization of Al in cross-sections along the root tip will contribute to support the hypothesis on Al binding stages and ligand exchange processes during symplastic radial Al transport in the root tip put forward by Klug and Horst (2010*b*).

Materials and methods

Plant material

Buckwheat (*Fagopyrum esculentum* Moench), cultivar 'Lifago' (Deutsche Saatveredelung AG, Lippstadt, Germany), was germinated in peat substrate containing 30% clay (Balster Einheitserdewerk GmbH, Fröndenberg, Germany). Plants were grown for 4 weeks in a greenhouse at 25/20 °C day/night temperatures. After this period of growth the shoots were cut 1 cm below the first node with adventitious root initials and additionally above the primary leaf to reduce transpiration. These shoot cuttings were transferred to low ionic strength nutrient solution with the following composition (μM): 500 KNO_3, 162 $MgSO_4$, 30 KH_2PO_4, 250 $Ca(NO_3)_2$, 8 H_3BO_3, 0.2 $CuSO_4$, 0.2 $ZnSO_4$, 5 $MnSO_4$, 0.2 $(NH_4)_6Mo_7O_{24}$, 50 NaCl, and 30 Fe-EDDHA for 4 d, keeping the shoots at 100% relative humidity (RH) until adventitious roots had emerged. The following day the plants were adapted to lower RH by reducing air humidification. After another day the pH of the nutrient solution was reduced in three steps to 4.3, resulting in at least 12 h for adaptation to the low pH before the beginning of the Al treatment. Afterwards, the plants were transferred to a simplified nutrient solution (500 μM $CaCl_2$, 8 μM H_3BO_3, 100 μM K_2SO_4, pH 4.3) supplemented with either 0 μM or 75 μM $AlCl_3$. A concentration of 75 μM $AlCl_3$ inhibits root growth between 50% and 60% (Klug and Horst, 2010*b*) and activates Al exclusion and tolerance mechanisms (Klug and Horst, 2010*a*). The pH was checked frequently and, when necessary, re-adjusted to 4.3 using 0.1 M HCl or 0.1 M KOH added drop-wise under vigorous stirring. The nutrient solution was aerated continuously. For comparison of the root radial distribution of Al in adventitious and primary root apices 3-day-old seedlings were exposed to 75 μM Al for 24 h in minimal nutrient solution containing 500 μM $CaCl_2$, 8 μM H_3BO_3, and 75 μM, pH 4.3 (see Supplementary Fig. S1 available at *JXB* online).

Staining of aluminium with fluorescent dyes

To clarify systematically the complex formation of Al with lumogallion and morin and to establish optimum staining conditions, either the Al concentration at a given dye concentration or the dye concentration at a given Al concentration was varied (Figs 2, 3). The Al–organic ligand solutions were incubated at 25 °C for 0.5 h. Morin [33 mM in dimethylsulphoxide (DMSO)] was added to a final concentration of 30 μM at pH 4.8. Lumogallion (1 mM in 0.1 M sodium acetate buffer, pH 5.2) was added to a final concentration of 30 μM lumogallion in the sample. The Al–dye complex formation was studied after incubation at 25 °C for 1 h under continuous shaking. After incubation the fluorescence was measured with a Hitachi spectrofluorometer (F2000, Hitachi Ltd, Tokyo, Japan). The fluorescence maxima of morin and lumogallion were determined by dye-specific wavelength scans to adjust the optimum excitation and emission wavelengths. Al–lumogallion and Al–morin fluorescences were determined at excitation/emission wavelengths of 507/567 nm and 418/502 nm, respectively.

Microscopy

Adventitious root tips of buckwheat plants treated with 75 μM Al for 24 h were excised 10 mm behind the root tip and immediately placed in chilled (4 °C), Al-free simplified nutrient solution (see above) for 10 min. Apical 0–5, 6–10, 11–15, 16–20, 21–25, and 26–30 mm adventitious root sections from plants treated with 75 μM Al for 0.25, 0.5, 1, 2, 4, 8, or 24 h were embedded in 5% (w/v) low-gelling point agarose (Fluka, Buchs, Switzerland) at 35 °C. These embedded root tips were free-hand sectioned using a razor blade. After sectioning, the slices were not washed, because preliminary comparisons revealed that washing led to Al redistribution on the cellular and tissue level. Slices of agarose-embedded root tips were placed on microscopy glass slides, and a drop of morin solution was placed on the agarose-embedded free-hand root tip sections. After an incubation time of 5 min, the sections were placed under a Zeiss Axioscope microscope (Zeiss, Axioscope, Jena, Germany), equipped with epifluorescence illumination (Mercury lamp, HBO 50 W). The filter settings were: band pass filter BP 395–440 nm (exciter), beam splitter FT 510 nm, and long-wave pass filter LP 515 nm (emitter) (Browne et al., 1990*b*). Pictures were taken with a digital camera (AxioVison, Zeiss, Jena, Germany).

Laser-ablation ICP-MS

For LA-ICP-MS, an additional experiment was carried out. Plants were treated for 24 h with 75 μM $AlCl_3$ in 18.0 l of simplified nutrient solution (500 μM $CaCl_2$, 8 μM H_3BO_3, 100 μM K_2SO_4, pH 4.3). Root tips were excised and sectioned in 5 mm segments (0–5, 6–10, 11–15, 16–20, 21–25, and 26–30 mm behind the tip). These segments were embedded in 5% (w/v) low-gelling point agarose (Fluka) at 35 °C. These embedded root tips were free-hand sectioned using a razor blade. Slices of agarose and embedded root tips were placed on microscopy glass slides. The

embedding of root tips in agarose served as protection against desiccation in the argon flow and, furthermore, represented an adequate physical fixation with regard to forces occurring during the laser ablation process. Tissues were ablated using a solid state NYAG-laser (UP193 SS, New Wave Research Co. Ltd, Cambridge, UK). The ^{13}C signal served as internal standard. ^{13}C and ^{27}Al signals were detected using the quadropole ICP-MS (7500 CX, Agilent Technologies, Santa Clara, CA, USA). The flow rate of the carrier gas and the make-up gas were adjusted to optimum output; the flow rate was 0.3 l min^{-1} for the carrier gas and 1.15 l min^{-1} for the make-up gas. Radio frequency power was set to 1300 W and the reaction mode was off. The laser parameters were set to 1.82 J cm^{-2} of output energy, 10 Hz repetition rate, 20 μm diameter of the crater size, and 20 μm s^{-1} scan speed.

For the calibration of the Al signal, a mixture of pectin and agar was used. The C content in the dry matter of 46% and a dry matter content of 2.9% were adjusted finally to match the conditions of freshly harvested adventitious buckwheat root tips. Al was added to the calibration mixture [0, 5, and 10 nmol (10 mm root tip)$^{-1}$] to simulate Al concentrations typically observed in root tips. After polymerization, slices were cut and placed on microscopy glass slides. Calibration was performed as described for the samples (see above). Every cross-section was visually captured by microscopy so that the individual diameter of each replicate could be determined by the laser ablation system software (Version 11) (New Wave Research Inc., Fremont, CA, USA). The diameter was sectored into four circular and one central region (Fig. 1). In the following these regions are termed: I, central cylinder; II, pericycle/endodermal; III; inner cortical; IV, outer cortical; and V, epidermal tissues.

Results

Morin and lumogallion showed increasing fluorescence intensities with increasing Al concentrations when recommended dye concentrations (30 μM morin; 60 μM lumogallion) were applied (data not shown). Both dyes stained Al highly effectively in the 1–10 μM concentration range.

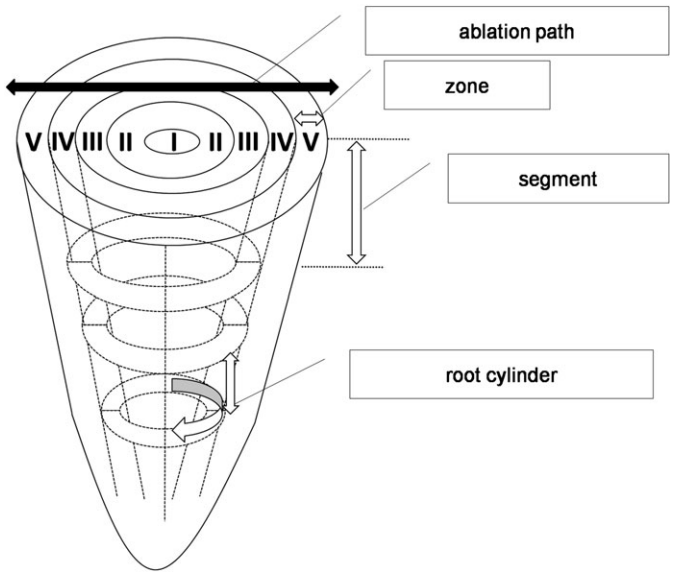

Fig. 1. Schematic overview over the laser ablation path across the root tip cross-section. The black arrow represents the diametric ablation path. White arrows represent specific zones, segments, and root cylinders as indicated in the text. I–V represent tissue areas with the same radial share of the whole radius.

However, variation in the dye concentrations at a given Al concentration, which yielded approximately the same fluorescence intensity for both dyes, showed an optimum curve for morin (Fig. 2A) with an optimum at 30 μM. The highest lumogallion fluorescence intensity was already measured at 10 μM. Further increasing the lumogallion concentration (10–40 μM) did not significantly change the fluorescence (Fig. 2B).

The effectiveness of both dyes to stain Al was tested by using a dye concentration of 30 μM (Fig. 3). Increasing the Al concentration increased the fluorescence intensity more steeply for morin than for lumogallion. Moreover, the fluorescence of the Al–morin complex responded to increasing Al concentrations up to 120 μM, whereas the maximum Al–lumogallion fluorescence was already reached at 50 μM Al. Therefore, morin showed higher fluorescence intensities than lumogallion irrespective of the Al concentration. The Al–morin fluorescence intensity significantly increased throughout the tested concentration range. However, lower Al than dye concentrations (3–10 μM) did not significantly differ in the case of morin but yielded significantly higher fluorescence intensities compared with lumogallion.

Al is known to be detoxified in Al-resistant and Al-accumulating plant species by organic acids, but the effectiveness of Al staining dyes in the presence of organic acids has not been systematically analysed, as yet. Therefore, the Al dye fluorescence in the presence of citrate, malate, and oxalate at different Al:ligand ratios was studied (Fig. 4). The fluorescence intensity of the Al–dye complex without any competing ligand was set to 100%. Oxalate at a ratio of 1:1 and particularly at 1:3 (Al:oxalate) reduced the fluorescence intensity of the Al–lumogallion complex more strongly than that of the Al–morin complex (Fig. 4). The presence of citrate greatly reduced the fluorescence intensity of both Al–dye complexes even at the 1:1 ratio. The presence of malate only reduced the fluorescence intensity of the Al–lumogallion complex but not that of the Al–morin complex. The presence of excess citrate concentrations reduced the Al–morin fluorescence by ~63%. The Al–lumogallion fluorescence was reduced by 76% compared with the maximum fluorescence of the dyes. The results indicate that, under these specific *in vitro* assay conditions, morin is more sensitive than lumogallion particularly in the presence of competing ligands such as oxalate and citrate.

Therefore, morin was used for Al *in situ* localization in buckwheat adventitious root tip cross-sections (Fig. 5). Only a very low autofluorescence was visible in the cross-sections not treated with Al (Fig. 5D). Morin staining of buckwheat root cross-sections after treatment with 75 μM Al from 0.5 h to 24 h revealed that Al could be detected across the whole cross-section as early as after 15 min of Al treatment (Fig. 6).

In Fig. 5 the localization of Al with morin in root sections at different distances from the root apex is shown. Relating the fluorescence intensity to Al concentrations across the root sections is not possible because, generally, the fluorescence intensity of the entire cross-sections decreased with increasing distance from the root apex.

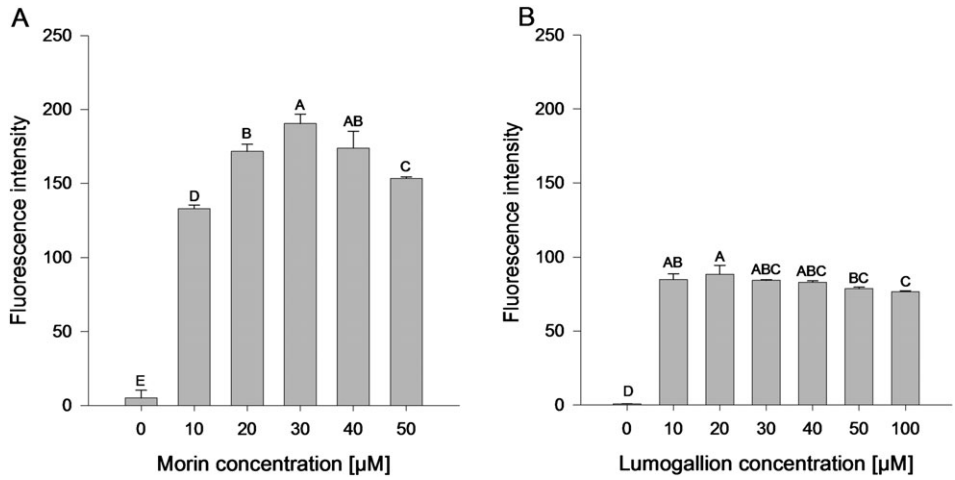

Fig. 2. Effect of morin and lumogallion concentrations on the fluorescence intensity at given Al concentrations. For morin (A) , 6 μM and for lumogallion (B) 3 μM $AlCl_3$ were added. Morin was measured at pH 4.8 at excitation and emission wavelengths of 418 nm and 502 nm, respectively. Lumogallion was measured at pH 5.2 in 0.1 M acetate buffer at excitation and emission wavelengths of 507 nm and 567 nm, respectively. Bars represent means ±SD, n=4. Different letters denote a significant difference (Tukey test P <0.05).

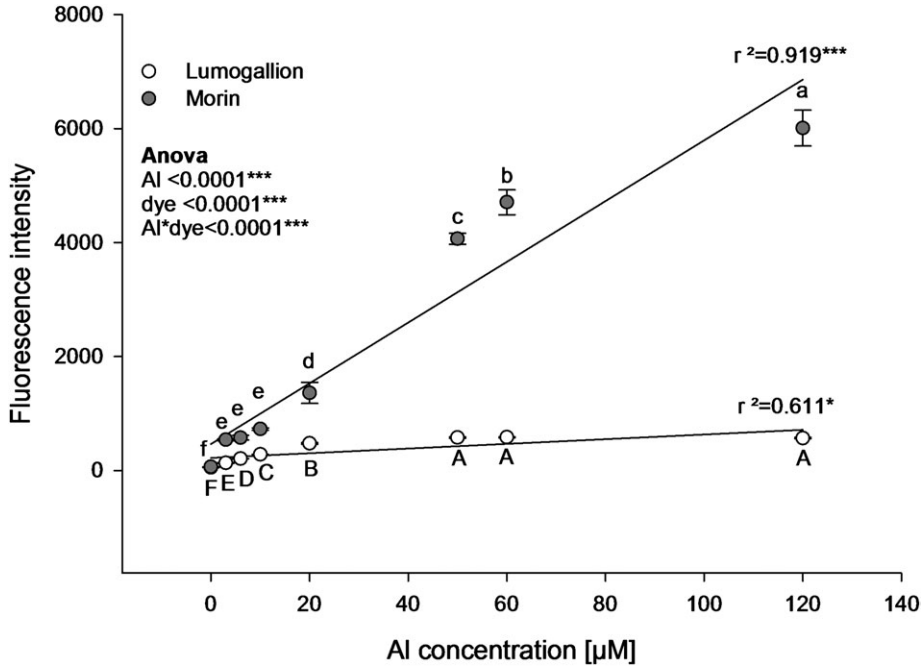

Fig. 3. Regression analysis of fluorescence intensities of Al–lumogallion and Al–morin complexes at a given dye concentration (30 μM) but varied Al concentrations. Al–lumogallion was measured at pH 5.2 in 0.1 M acetate buffer at excitation and emission wavelengths of 507 nm and 567 nm, respectively. Al–morin was measured at pH 4.8 at excitation and emission wavelengths of 418 nm and 502 nm, respectively. Symbols represent means ±SD, n=4. Morin samples at 50, 60, and 120 μM Al were diluted appropriately to remain in the effective measuring range. Different letters denote a significant statistical difference (Tukey test P <0.05). Upper case letters denote the comparison between different Al–lumogallion fluorescence intensities. Lower case letters denote the comparison between different Al–morin fluorescence intensities.

Therefore, when taking the micrographs, the exposure times were prolonged with decreasing fluorescence intensity (Fig. 5C) to allow the best comparison of the fluorescence distribution within a cross-section.

After 0.5 h Al treatment (Fig. 6) as well as after 24 h Al treatment, Al was located particularly in the epidermis and outer cortical cells in the apical 0–5 mm segment (Fig. 5A). Most of the stained Al was located in the symplast (Fig. 5B, yellow arrows). Only intact cells could be stained, indicating that Al was located predominantly in the cytosol, which represents the majority of the total cell volume in apical root tip cells. Empty cells (white arrows) did not show fluorescence, suggesting that cell walls did not contain Al, or morin was not able to stain cell-wall bound Al.

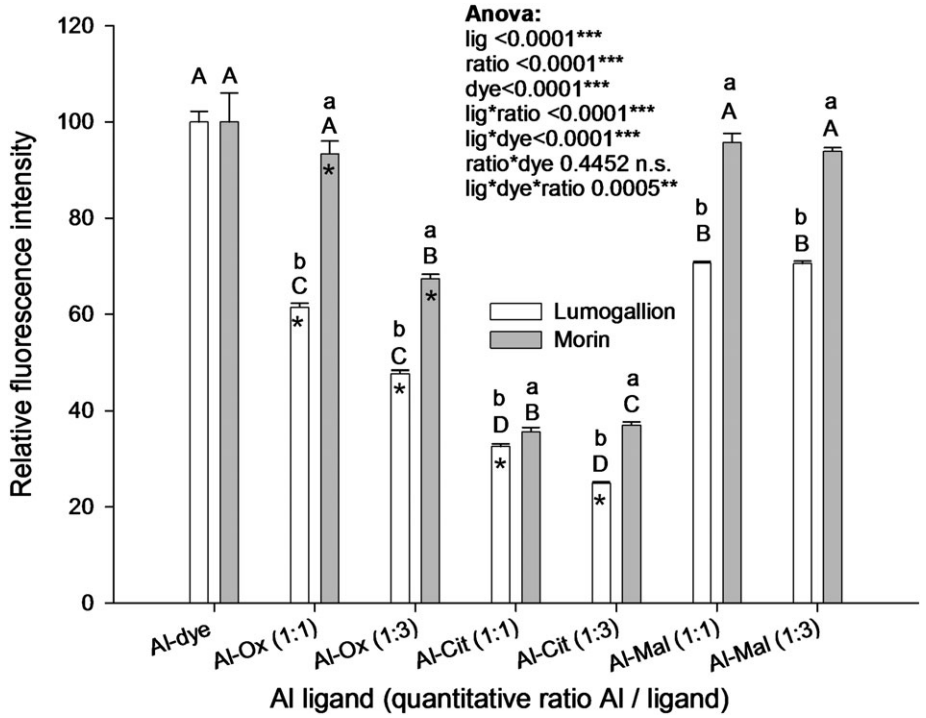

Fig. 4. Relative fluorescence intensity of lumogallion and morin as affected by the presence of the Al-chelating ligands oxalate, citrate, and malate in different ratios. Morin: $AlCl_3$ 6 μM, morin 30 μM, organic acids 6 μM or 18 μM, pH 4.8; detection at excitation and emission wavelengths of 418 nm and 502 nm, respectively. Lumogallion: $AlCl_3$ 20 μM, lumogallion 60 μM, organic acids 20 μM or 60 μM, buffered by sodium acetate buffer pH 5.2; detection at excitation and emission wavelengths of 507 nm and 567 nm, respectively. Bars represent means ±SD; n=4. Different letters denote significant statistical differences (Tukey test P <0.05). Upper case letters denote the comparison between different ligands within one dye and one ratio. Lower case letters denote the comparison between lumogallion and morin within one ligand and one ratio. The asterisks mark significant differences between different ratios within one dye and one ligand.

The 6–10 mm segment was rather uniformly stained across the whole root section. Also in this segment Al was predominantly symplastically located. With increasing distance from the root tip, the vacuole comprises the major share of the total cell volume; however, the vacuole shows almost no fluorescence. The fluorescence is primarily found in a cytoplasmatic ring surrounding the vacuole. In the 11–15 mm root segment the most pronounced Al–morin fluorescence intensity was located in stelar and endodermal root tip tissues. Generally, the fluorescence contribution of the epidermal layers relative to the total fluorescence of a cross-section decreased with increasing distance from the root tip. This Al distribution pattern did not change much in the 16–20 mm segment. In the following 21–25 mm and 26–30 mm root segments, the xylem vessels in particular exhibited marked Al–morin fluorescence. In the 21–25 mm segment, the first lateral roots emerged in the majority of the observed cross-sections. Compared with distal primary root tissues these lateral root tips were stained more intensively. The tissue surrounding the lateral roots, particularly the endodermal perforation, did not show enhanced fluorescence intensity (the insert in the 26–30 mm segment micrograph shows an area where the endodermis is penetrated). This suggests that either apoplastic by-pass flow plays a minor role or Al is bound in complexes with morin which are not detectable.

The segments which showed a marked difference in the Al–morin fluorescence distribution were analysed using a kinetic approach with increasing treatment durations at a constant exposure time of 380 ms (Fig. 6). The increasing fluorescence from short-term (0.25 h) to long-term Al treatment (8 h) indicated increasing Al concentrations especially in the 5–10 mm segments. The kinetic analysis revealed comparable trends to those obtained after 24 h of Al treatment. The segment at a distance of 5–10 mm from the root tip showed a homogenous radial distribution of Al. The entire cortex is uniformly stained by morin already after 15 min Al treatment. From 1 h onwards the cortex and the central cylinder exhibited a uniform fluorescence intensity, suggesting that in the 5–10 mm segment Al penetrates the whole root diameter. In the adjacent 10–15 mm segment the Al–morin fluorescence is not homogenously distributed. The epidermal cell layer always showed a bright fluorescence; the cortical cells did not show a marked fluorescence. After 4 h Al treatment the vascular bundles in the stelar tissues exhibited a distinct fluorescence, becoming intensified after 8 h Al treatment, suggesting that Al localized in the vascular bundles is transported into this segment from more apical segments.

The radial distribution of Al along the root apex of the much thinner primary roots was principally similar compared with adventitious roots (Supplementary Fig. S1 at *JXB* online) in

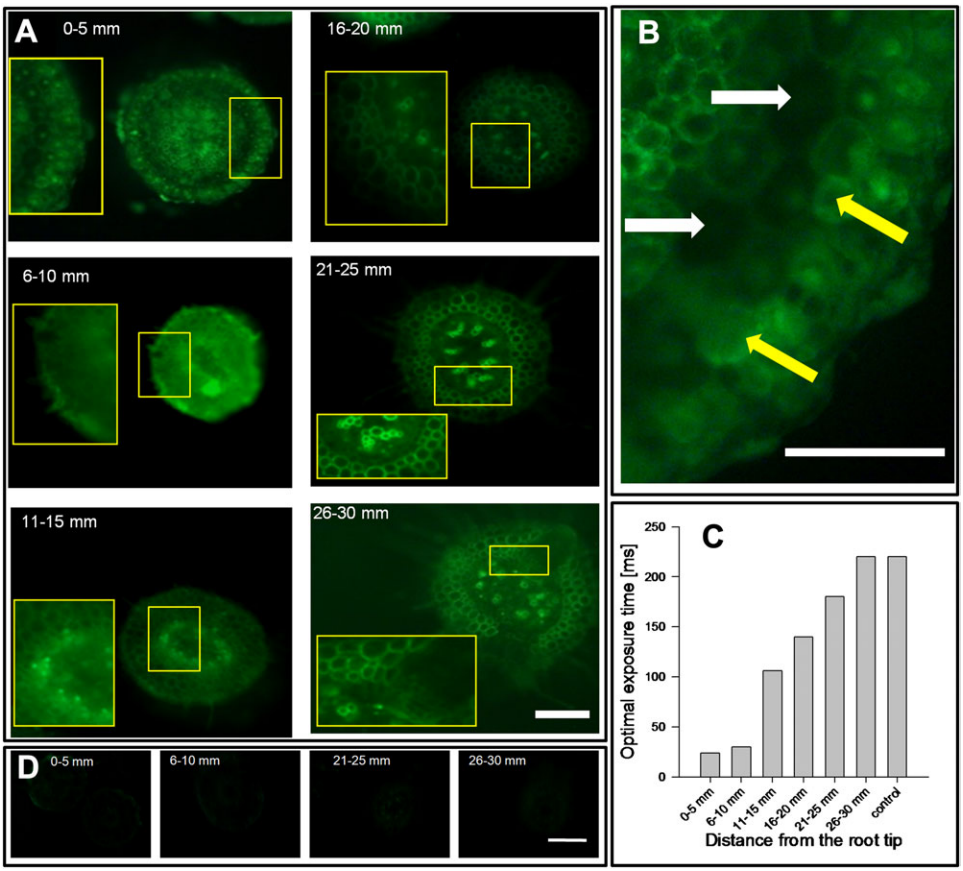

Fig. 5. (A) Fluorescence images of the Al–morin complex in buckwheat root tip cross-sections at an increasing distance from the root tip. Inserts (larger squares) show close-ups of the marked area (smaller squares). Intact root tips were grown in simplified nutrient solution (500 μM $CaCl_2$, 100 μM K_2SO4, 8 μM H_3BO_3, pH 4.3 with 75 μM $AlCl_3$ for 24 h). The scale bar represents 200 μm at 100-fold magnification. (B) Close-up of the 0–5 mm cross-section. Yellow arrows indicate cells with intact cytoplasm showing high symplastic fluorescence intensities; white arrows indicate damaged and thus empty cells. Scale bars represents 100 μm at 200-fold magnification. (C) Optimal exposure time measured by Axiovison software (Carl Zeiss Micro Imaging GmbH, Göttingen, Germany) reflecting decreasing Al contents with increasing distance from the root apex. (D) Representative cross-sections of the control treatment (0 μM Al, 24 h) with increasing distance from the root tip stained by morin. The scale bar represents 200 μm at 100-fold magnification.

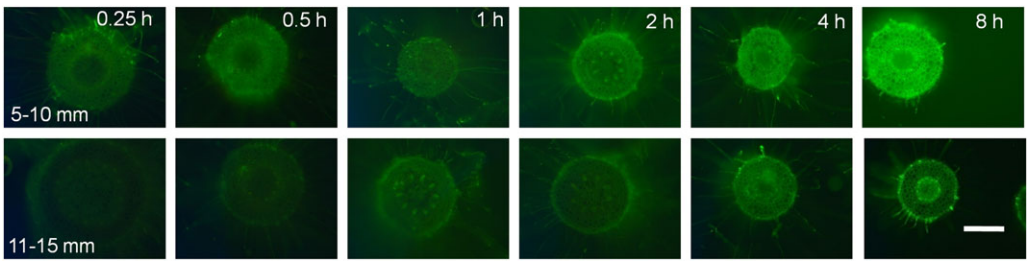

Fig. 6. Root tip cross-section at a distance of 5–10 mm (upper row) and 11–15 mm (lower row) from the root tip after 0.25, 0.5, 1, 2, 4, and 8 h treatment duration in simplified nutrient solution (500 μM $CaCl_2$, 100 μM K_2SO_4, 8 μM H_3BO_3, 75 μM $AlCl_3$, pH 4.3). The scale bar represents 100 μm at 100-fold magnification.

the root cortex. However, the Al–morin fluorescence intensity in the stele of primary roots was too low to reach any conclusions on Al distribution in this tissue and on xylem Al transport. This may be due to the small diameter of these primary root tips allowing only a much smaller loading of Al into the central cylinder and the xylem below the Al detection limit.

Since the information about the Al distribution in root tip sections as obtained by morin staining is only qualitative and does not include Al not stainable by morin (cell wall) LA-ICP-MS was applied for the quantitative localization of Al. Figure 7 shows a representative Al quantification pattern expressed as the Al signal intensity in a root cross-section at distances of 0–5 mm (Fig. 7A) and 11–15 mm (Fig. 7B) from the root tip. This signal intensity was calibrated (see Materials and methods) and calculated as either Al concentration (Fig. 8, left column) or Al content (Fig. 8, right column). The latter was

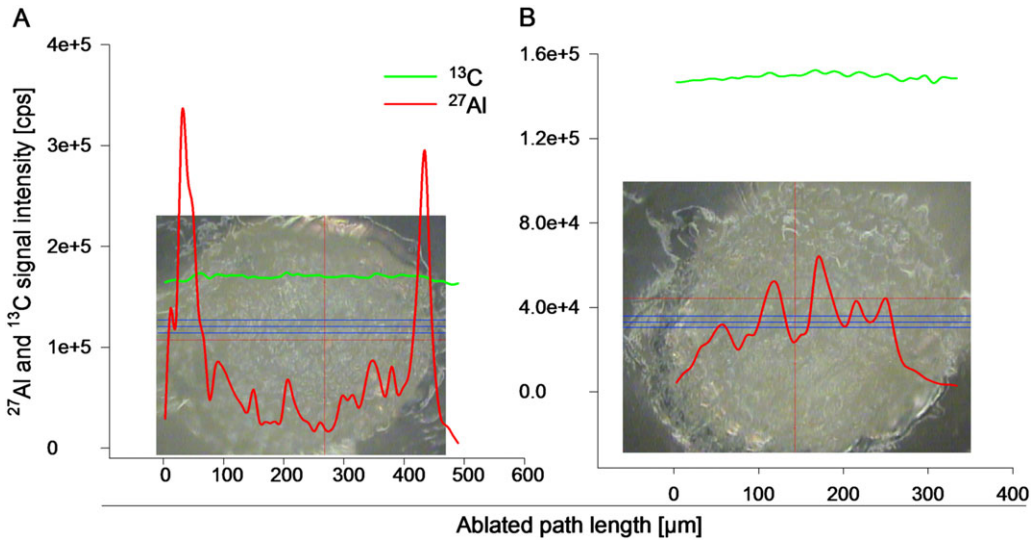

Fig. 7. ^{27}Al and ^{13}C signal intensities of a representative root cross-section prepared from the 0–5 mm (A) and 11–15 mm (B) zone after 24 h treatment with 75 µM Al in minimal nutrient solution (500 µM $CaCl_2$, 100 µM K_2SO_4, 8 µM M H_3BO_3, pH 4.3). The red line represents the ^{27}Al; the green line the ^{13}C (internal standard) signal intensities. The triple blue line represents the ablated path. The laser beam was adjusted to a diameter of 20 µm and 50% energy, resulting in 1.82 J cm^{-1}.

extrapolated by the geometric volume of four hollow cylinders and one central cylinder (see Fig. 1). Therefore, the root diameter of each root cross-section was divided by nine, resulting in four circular zones and one central zone (see Fig. 1) which can be roughly assigned to the epidermal layer, outer and inner cortical layer, endodermal layer, and stelar tissue. By including the ^{13}C signal as the internal calibrator, the ^{27}Al signal was normalized to the amount of cell material ablated by the laser beam which may be affected by different cell layer densities or tissue colours along the ablation path. Both cross-sections showed a uniform ^{13}C signal intensity, confirming the suitability of this signal for the normalization of the ^{27}Al signal (Fig. 7). Cross-sections prepared from the apical root tip (0–5 mm) showed high ^{27}Al signal intensities in the epidermal and outer cortical cell layer, and lower intensities in the inner root tip tissues. In contrast, in the 11–15 mm root tip segment, the highest ^{27}Al intensities were found in stelar root tip tissues, whereas the outer cell layers exhibited low intensities.

Using the described calibration method and the normalized ^{27}Al signals, the Al concentrations in the root tissue volume and the Al contents of the root section cylinders were calculated (Fig. 8) for individual root tissue zones. There were statistically significant differences between the Al concentrations and Al contents within individual tissues and along the root axis. At the root tip, the segment (0–5 mm) was characterized by high Al concentrations in the epidermal and outer cortical cell layers (Fig. 8). This Al distribution pattern changed in the adjacent 5 mm zone (6–10 mm) to a more homogenous Al distribution. In the 11–15 mm section, the highest Al concentration was found in the stelar tissue and tended also to be higher in the endodermal layer. This distribution was also found in the 16–20 mm zone, where the elevated Al concentration at the endodermis became more pronounced. The two following segments were characterized by low and more homogenously distributed Al with slightly lower Al concentrations in the outer than in the inner root tissue layers.

The analysed Al concentrations (Fig. 8, left column) were multiplied by the volumes of the previously defined tissue zones (I–V, see Fig. 1) to yield Al contents of these root tissue cylinders. When comparing the Al contents it has to be considered that the volumes of the individual root cylinders from zone V to zone I differ from 39.5, 29.6, 19.8, 9.9, to 1.2% of the total volume, respectively. In the apical 0–5 mm root segment a steep gradient in Al contents existed from the outer to the inner cell layers, reflecting the higher share of the volume and the concentration gradient. With increasing distance from the root apex the gradient between outer and inner cortical root tissues disappeared, showing that the increasing concentrations in inner tissues compensate for their lower share of the volume. The stele (zone I) always showed the lowest Al content because of its small share of the volume in spite of the high Al concentrations particularly in the 11–15 mm root zone.

Comparing the total Al contents of the root zones along the root axis (numbers in Fig. 8, right column), a decreasing gradient from the root apex to the more basal root zone is apparent.

Discussion

Knowledge of the binding stages and stability constants of dye complexes is a prerequisite for qualitative and semi-quantitative statements about the Al distribution within plant tissues. A spectrofluorometric determination of specific Al species by a complex-specific shift of emitted wavelength spectra failed to provide information about Al–ligand interactions (Brauer, 2001). Both morin and lumogallion are known to detect Al

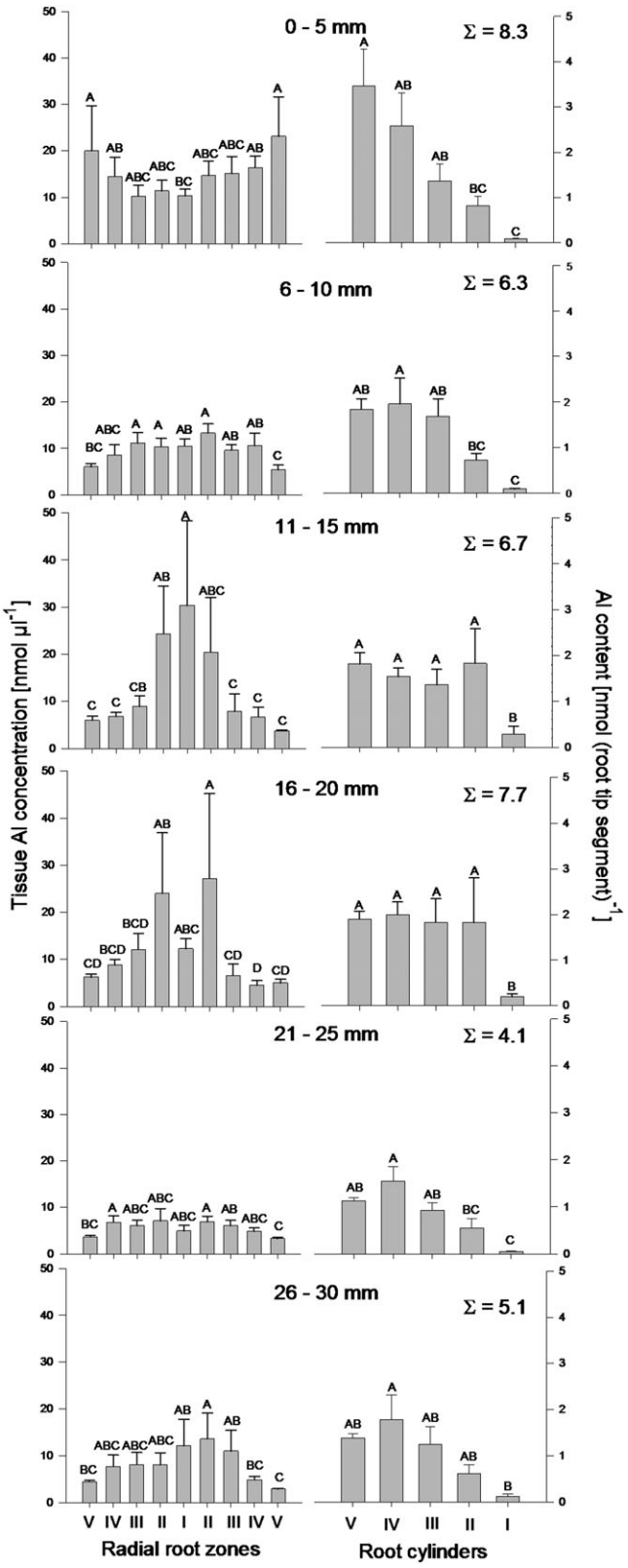

Fig. 8. Al concentrations (left column) along a buckwheat adventitious root, and Al contents of the 5 mm root segment cylinders (right column, root cylinders I–V, see Fig. 1) at different distances from the root tip as determined by LA-ICP-MS. The plants were treated with 75 µM $AlCl_3$ for 24 h in simplified nutrient solution (500 µM $CaCl_2$, 100 µM K_2SO_4, 8 µM H_3BO_3, pH 4.3). Root tip tissue layers were defined by dividing the root diameter into nine even regions. Data were calibrated by ablation of an agarose–pectin mixture with the same carbon and water contents as buckwheat root tips and defined Al concentrations. The Al signal intensity was normalized using the ^{13}C signal intensity and calculated as the mean over the ablated path length of 10 µm and 1 s ablation time. Bars represent means of six ablated cross-section diameters of six different root tips per 5 mm segment. Different letters denote significant statistical differences between root zones/root cylinders (Tukey test P <0.05).

with high sensitivity, but information on their specific staining efficiencies of complexed Al is currently inconsistent. The lumogallion staining method was reported to be more sensitive for Al detection than the use of morin according to a confocal microscopic study (Kataoka *et al.*, 1997). In contrast, in this study, the morin staining method showed a higher sensitivity. However, Al–lumogallion was reported to have a high stability constant (log k 7.76) over the pH range from 2 to 5.7 (Shuman, 1992), whereas the stability constant of the Al–morin complex was reported to be lower (log k of 6.47). Unfortunately, in that study, the effect of pH was not further specified (Katyal and Prakash, 1977). Later, Saarl and Steltz (1983) showed a clear pH dependency of Al–morin complex formation and fluorescence intensity, which might explain the discrepancy in stability constants and underestimation of the Al–morin stability under certain conditions. Differences in the sensitivity of both dyes may result from the coordination chemistry of the Al–dye complex formation.

The Al–morin complex had increased fluorescence emission when the Al:morin ratio was switched from 1:1 to 1:3. Thus, one Al ion can be complexed by one, two, or even three molecules of morin, thereby gradually increasing the fluorescence intensity of the complex. However, on exceeding the 1:3 ratio the fluorescence intensity decreases. In contrast, lumogallion exhibited the maximal fluorescence intensity at a 1:1 concentration ratio indicating that lumogallion binds Al exclusively at a ratio of 1:1.

Lumogallion has been shown to detect Al even in the presence of organic ligands (Shuman, 1992; Sutheimer and Cabaniss, 1995). Contradictory results (on the one hand morin stains Al more efficiently than lumogallion, on the other hand morin is not able to form a complex with Al in the presence of organic acid anions) led to a series of tests being conducted to clarify the competitiveness of each dye to stain Al in the presence of Al-complexing carboxylic acid anions. Under the current microscope set-up, morin emitted higher fluorescence intensities than lumogallion (Fig. 2). Furthermore, the presence of oxalic, malic, or citric acid anions reduced the fluorescence intensity of Al–morin less than that of Al–lumogallion (Fig. 3). Generally, the fluorescence formation of Al–morin complexes in the presence of organic acid ligands reflects the stability constants of Al–organic anion complexes (Stevenson and Vance, 1982; Martin, 1994): Al–$Cit_{(1:1)}$ (lowest fluorescence/highest stability) >Al–$Ox_{(1:3)}$ >Al–$Ox_{(1:1)}$ >Al–Mal (most intense fluorescence/lowest stability). The autofluorescence of the individual dyes alone was negligible (<5%). Therefore, it is concluded

from these results that the use of morin is an appropriate method to track Al on its symplastic way through the root cortex in buckwheat where Al is symplastically detoxified and transported as an oxalate complex into the stele. The staining of Al by morin in the central cylinder and the xylem may, however, greatly underestimate the Al concentration, because, here, Al is complexed by citrate (Ma and Hiradate, 2001; Klug and Horst, 2010*a*, *b*).

In this study, an LA-ICP-MS-based method was developed for the determination of total Al in root cross-sections. The method was calibrated using Al standards in an agarose–pectin matrix to transform ^{27}Al intensities into Al concentrations. The reliability of this calibration can be verified by comparing the Al contents of root tips based on conventional total Al determination using graphite furnace atomic absorption spectrometry after acid digestion of the root tissue with the calculated Al contents based on the LA-ICP-MS measurements of cross-sections of specific root segments. Analysing the Al contents of 1 mm apical root segments, Al contents of ~20 nmol and 10 nmol were measured for the first and second 5 mm of the root tip, respectively (Klug and Horst, 2010*a*; Fig. 2) which was higher than the calculated 8.3 nmol and 6.3 nmol Al content of the apical and subapical 5 mm segments, respectively, using LA-ICP-MS (Fig. 8, right column). However, if it is considered that the LA-ICP-MS measurements were made at more basal cross-sections of the respective 5 mm segments, measured and calculated Al contents compare fairly well. Also the measured tissue Al concentrations can be compared: the LA-ICP-MS-measured tissue Al concentration averaged over the apical and subapical two 5 mm segments and the radial root tissues were 12.3 nmol μl^{-1} (Fig. 8, left column). After the same 24 h Al treatment period the cytosolic Al concentration of the 10 mm root apex was 7 mM (corresponding to 7 nmol μl^{-1}) (Klug and Horst, 2010*b*; Fig. 2). However, the cytosolic Al represented only about one-third of the total Al (Klug and Horst, 2010*b*; Fig. 3). Thus, the measured tissue Al concentrations also compared fairly well and confirm the reliable calibration of the Al contents measured by LA-ICP-MS.

In buckwheat Al is readily translocated to above-ground plant organs (Ma and Hiradate, 2000; Shen *et al.*, 2006). As a prerequisite, Al needs to be rapidly transferred from the root surface through the root cortex to the stelar tissues. The analysis of Al uptake and translocation indicated the importance of spatial differences between apical root sections in Al uptake and Al xylem loading in buckwheat (Klug and Horst, 2010*a*). These authors concluded from their study that Al is primarily accumulated in the 10 mm apical segment of the root tip, while the subapical 10–20 mm segment was characterized by the highest activity of Al loading of the xylem.

To better understand the mechanism of Al transport, in the present study special emphasis was placed on the root radial Al localization along the root apex using morin in comparison with total Al. Al primarily accumulated in the outer cortical layers of the root apex (0–5 mm) (see Figs 5A, 6, 7A, 8). Additionally, based on fluorescence intensity this section showed the highest contribution of symplastic to total Al–morin fluorescence (Fig. 5A) irrespective of the treatment duration (Fig. 6). This constant Al distribution suggests an equilibrium between Al accumulation and export to the adjacent basal root segment and thus supports the suggestions made by Klug and Horst (2010*a*) that Al is taken up primarily at the apical root tip. The intense staining by morin in this root segment also confirms that Al is, to a large extent, present in a soluble, morin-stainable binding stage in the cytosol [mostly Al–oxalate in buckwheat (Klug and Horst, 2010*b*)] and not predominantly firmly bound to the cell wall as shown for the Al excluder common bean (Eticha *et al.*, 2005; Rangel *et al.*, 2009). In segment 1 (0–5 mm) and segment 2 (6–10 mm) the root radial distribution of Al according to morin staining (Fig. 5A) and LA-ICP-MS (Fig. 8) showed comparable results. Also in the segments 11–15 mm and 16–20 mm both methods revealed a similar radial Al distribution, with the highest Al concentrations in the central cylinder and the pericycle/endodermal tissue. However, in spite of a very high Al tissue concentration measured by LA-ICP-MS, the fluorescence intensity was low (see much higher exposure time necessary for the segments 11–20 mm, Fig. 5C). This indicates that the Al–morin staining underestimates the Al concentrations in these tissues which could be expected, because in these tissues citrate is the dominant organic acid anion (Klug and Horst, 2010*b*). As shown in Fig. 4, Al complexation by citrate greatly reduces the Al staining by morin.

It is known that the xylem parenchyma cells are primarily responsible for xylem loading of ions for long-distance transport (Köhler and Raschke, 2007). Furthermore, it was shown that specific transporters, for example the boron transporter BOR1, are restricted to pericycle cells (Takano *et al.*, 2002). Pericycle cells comprise the outermost part of the stele, which showed bright Al morin fluorescence in the segments 11–20 mm (Fig. 5) and the highest Al concentrations (Fig. 8) in the present study, suggesting that these cells in this root zone may play a key role in xylem loading of Al in buckwheat roots. The loading of Al into the xylem in the root segment 10–20 mm leads to intensive Al–morin fluorescence of single xylem vessels in more basal root segments (20–30 mm) (Fig. 5).

In conclusion, the presented results show that the staining of Al with morin is an appropriate means to study qualitatively the radial Al distribution along the root tip axis in buckwheat. The results compare well with the distribution of total Al determined by LA-ICP-MS. This is attributed to the fact that a substantial part of the Al in buckwheat roots is complexed by organic acid anions which do not prevent Al–morin complex formation. The results support the view that the 10 mm apical root tip is the main site of Al uptake in the symplast of the root cortex, while the subapical 10–20 mm zone is the main site of xylem loading through the pericycle and xylem parenchyma cells. Progress in the better molecular understanding of Al transport in the Al accumulator buckwheat will depend on the consideration of the tissue specificity of Al transport and complexation.

Supplementary data

Supplementary data are available at *JXB* online.

Figure S1. Aluminium distribution in cross-sections of primary root tips after 24 h Al treatment in minimal nutrient

solution containing 500 μM $CaCl_2$, 8 μM H_3BO_3, and 75 μM $AlCl_3$ at pH 4.3 at a distance of 0–30 mm from the root tip.

References

Ahn SJ, Sivaguru M, Chung GC, Rengel Z, Matsumoto H. 2002. Aluminium-induced growth inhibition is associated with impaired efflux and influx of H^+ across the plasma membrane in root apices of squash (*Cucurbita pepo*). *Journal of Experimental Botany* **53,** 1959–1966.

Babourina O, Rengel Z. 2009. Uptake of aluminium into Arabidopsis root cells measured by fluorescent lifetime imaging. *Annals of Botany* **104,** 189–195.

Brauer D. 2001. Rapid inhibition of root growth in wheat is associated with aluminum uptake as followed by changes in morin fluorescence. *Journal of Plant Nutrition* **24,** 1243–1253.

Browne BA, McColl JG, Driscoll CT. 1990. *a*. Aluminum speciation using morin: I. Morin and its complexes with aluminum. *Journal of Environmental Quality* **19,** 65–72.

Browne BA, Driscoll CT, McColl JG. 1990. *b*. Aluminum speciation using morin: II. Principles and procedures. *Journal of Environmental Quality* **19,** 73–82.

Eticha D, Staß A, Horst WJ. 2005. Localization of aluminium in the maize root apex: can morin detect cell-wall bound aluminium? *Journal of Experimental Botany* **56,** 1351–1357.

Gutierrez AC, Gehlen MH. 2002. Time resolved fluorescence spectroscopy of quercetin and morin complexes with Al^{3+}. *Spectrochimica Acta Part A* **58,** 83–89.

Jones DL, Blancaflor EB, Kochian LV, Gilroy S. 2006. Spatial coordination of aluminium uptake, production of reactive oxygen species, callose production and wall rigidification in maize roots. *Plant, Cell and Environment* **29,** 1309–1318.

Kataoka T, Iikura H, Nakanishi TM. 1997. Aluminum distribution and viability of plant root and cultured cells. *Soil Science and Plant Nutrition* **43,** 1003–1007.

Katyal M, Prakash S. 1977. Analytical reactions of hydroxy flavones. *Talanta* **24,** 367–375.

Klug B, Horst WJ. 2010*a*. Spatial characteristics of aluminium uptake and translocation in roots of buckwheat (*Fagopyrum esculentum* Moench). *Physiologia Plantarum* **139,** 181–191.

Klug B, Horst WJ. 2010*b*. Oxalate exudation into the root-tip water free space confers protection from Al toxicity and allows Al accumulation in the symplast in buckwheat (*Fagopyrum esculentum*). *New Phytologist* **187,** 380–391.

Köhler B, Raschke K. 2007. Loading of ions into the xylem of the root. In: Sattelmacher B, Horst WJ, eds. *The apoplast of higher plants: compartment of storage, transport and reactions. The significance of the apoplast for the mineral nutrition of higher plants*. Dordrecht, The Netherlands: Springer, 181–200.

Levesque L, Mizzen CA, McLachlan DR, Fraser PE. 2000. Ligand specific effects on aluminum incorporation and toxicity in neurons and astrocytes. *Brain Research* **877,** 191–202.

Lian HZ, Kang YF, Bi S, Yasin A, Shao DL, Chen YJ, Dai LM, Tian LC. 2003. Morin applied in speciation of aluminium in natural waters and biological samples by reversed-phase high-performance liquid chromatography with fluorescence detection. *Analytical and Bioanalytical Chemistry* **376,** 542–548.

Ma JF, Hiradate S. 2000. Form of aluminium for uptake and translocation in buckwheat (*Fagopyrum esculentum* Moench). *Planta* **211,** 355–360.

Ma JF, Hiradate S, Matsumoto H. 1998. High aluminum resistance in buckwheat II. Oxalic acid detoxifies aluminum internally. *Plant Physiology* **117,** 753–759.

Martin RB. 1994. Aluminum: a neurotoxic product of acid rain. *Accounts of Chemical Research* **27,** 204–210.

Rangel AF, Rao IM, Horst WJ. 2009. Intracellular distribution and binding state of aluminum in root apices of two common bean (Phaseolus vulgaris) genotypes in relation to Al toxicity. *Physiologia Plantarum* **135,** 162–173.

Saarl LA, Seitz WR. 1983. Immobilized morin as fluorescence sensor for determination of aluminium (III). *Analytical Chemistry* **55,** 667–670.

Shen RF, Chen RF, Ma JF. 2006. Buckwheat accumulates aluminum in leaves but not in seeds. *Plant and Soil* **284,** 265–271.

Shuman MS. 1992. Dissociation pathways and species distribution of aluminum bound to an aquatic fluvic acid. *Environmental Science and Technology* **26,** 593–598.

Stevenson FJ, Vance GF. 1982. Naturally occurring aluminium–organic complexes. In: Martell AE, Smith RM, eds. *Critical stability constants*. New York: Plenum Press, 117–147.

Sutheimer SH, Cabaniss SE. 1995. Aqueous Al(III) speciation by high-performance cation exchange chromatography with fluorescence detection of the aluminum–lumogallion complex. *Analytical Chemistry* **67,** 2342–2349.

Takano J, Noguchi K, Yasumori M, Kobayashi M, Gajdos Z, Miwa K, Hayashi H, Yoneyama T, Fujiwara T. 2002. *Arabidopsis* boron transporter for xylem loading. *Nature* **420,** 337–340.

Tanoi K, Hayashi Y, Iikura H, Nakanishi M. 2001. Aluminum detection by lumogallion staining method in plants. *Analytical Science* **17,** 1455–1458.

Taylor GJ, McDonald-Stephens JL, Hunter DB, Bertsch PM, Elmore D, Rengel Z, Reid RJ. 2000. Direct measurement of aluminum uptake and distribution in single cells of *Chara corallina*. *Plant Physiology* **123,** 987–996.

Ščančar J, Milačič R. 2006. Aluminium speciation in environmental samples: a review. *Analytical and Bioanalytical Chemistry* **386,** 999–1012.

Vitorello VA, Haug A. 1997. An aluminum–morin fluorescence assay for the visualization and determination of aluminum in cultured cells of *Nicotiana tabacum* L. cv. BY-2. *Plant Science* **122,** 35–42.